

Lyman Continuum Escape Fraction in Ly α Emitters at $z \simeq 3.1$

Fuyan Bian¹★, Xiaohui Fan²

¹European Southern Observatory, Alonso de Córdova 3107, Casilla 19001, Vitacura, Santiago 19, Chile

²Steward Observatory, University of Arizona, 933 N Cherry Ave., Tucson, AZ 85721, USA

Accepted XXX. Received YYY; in original form ZZZ

ABSTRACT

We measure the LyC escape fraction in 54 faint Lyman Alpha Emitters (LAEs) at $z \simeq 3.1$ in the GOODS-South field. With the average magnitude of $R = 26.7$ AB ($M_{UV} = -18.8$, $L \simeq 0.1L^*$), these galaxies represent a population of compact young dwarf galaxies. Their properties are likely to resemble those in the galaxies responsible for reionising the Universe at $z > 6$. We do not detect LyC emission in any individual LAEs in the deep *HST* F336W images, which covers the rest-frame 820Å. We do not detect the LyC emission of these LAEs in the stacked F336W images, either. The 3σ upper limit of LyC escape fractions is $f_{\text{esc}} < 14 - 32\%$. However, the high Ly α rest-frame equivalent width, low stellar mass and UV luminosity of these LAEs suggest that they should have $f_{\text{esc}} > 50\%$. The low LyC escape fraction from this work and other stacking analysis suggest that the LyC leaking galaxies with $f_{\text{esc}} > 50\%$ at $z = 2 - 3$ do not follow the relation between the f_{esc} and UV luminosity and Ly α equivalent width (EW) derived from typical galaxies at similar redshift. Therefore, the UV luminosity and Ly α equivalent width (EW) are not the best indicators for the LyC escape fraction.

Key words: cosmology; dark ages, reionisation, first stars – galaxies; high-redshift

1 INTRODUCTION

The epoch of reionisation is a period when neutral hydrogen in the intergalactic medium (IGM) was ionised by the first generation energetic sources in the Universe. Current observations have relatively well constrained the cosmic reionisation history, which occurred at the redshift of $z = 7 - 10$ and finished largely by $z = 6$ (e.g. Fan et al. 2006a,b; Stark et al. 2011; Schroeder et al. 2013; Schenker et al. 2014; Bian et al. 2015; Bouwens et al. 2015b; Robertson et al. 2013; Planck Collaboration et al. 2016; Bañados et al. 2018; Itoh et al. 2018). However, it is still under debate what are the major sources that reionise the Universe due to the following two main uncertainties: (1) the faint-end luminosity function of star forming galaxies (e.g. Atek et al. 2018; Bouwens et al. 2017) and active galactic nuclei (AGN) (e.g., Giallongo et al. 2015; McGreer et al. 2018; Boutsia et al. 2018; Matsuoka et al. 2018) at high redshift, and (2) Lyman continuum (LyC) escape fraction (f_{esc}) in galaxies, the fraction of the ionising photons ($< 912\text{Å}$) that can escape from a galaxy to reach the IGM. If star-forming galaxies are the major sources to reionise the Universe, it requires a LyC escape fraction at least $f_{\text{esc}} = 0.2$

at the epoch of reionisation (e.g., Robertson et al. 2013; Naidu et al. 2019), by adopting a typical IGM clumping factor (e.g., Pawlik et al. 2009), galaxy luminosity function at $z = 7$ (e.g., Atek et al. 2015, 2018; Bouwens et al. 2015a, 2017; Livermore et al. 2017), and LyC photon production efficiency (e.g., Bouwens et al. 2016; Tang et al. 2018; Chevallard et al. 2018).

However, LyC escape fraction can not be directly measured in galaxies beyond $z = 4.5$ due to the high opacity of the IGM to LyC ionising photons (e.g., Vanzella et al. 2018). Thus we have to infer the LyC escape in the galaxies at the epoch of the reionisation based on either directly measuring LyC escape fraction in galaxies at lower redshift or correlating galaxy spatial positions with the Lyman alpha forest at $z > 6$ (e.g., Kakiichi et al. 2018). In the last decade, people have conducted extensive studies of LyC escape fraction in galaxies at $z < 4$ using a number of different approaches, including the rest-frame ultraviolet spectroscopy (e.g., Leitet et al. 2013; Leitherer et al. 2016; Izotov et al. 2016b,a; Steidel et al. 2001, 2018; Shapley et al. 2006, 2016; Nestor et al. 2013) and narrow/intermediate/broad-band UV imaging (e.g., Siana et al. 2007, 2015; Vanzella et al. 2010, 2016; Nestor et al. 2011; Cooke et al. 2014; Rutkowski et al. 2016, 2017; Vasei et al. 2016; Bian et al. 2017; Japelj et al.

★ E-mail: fbian@eso.org (FB)

2017; Naidu et al. 2017; Fletcher et al. 2018; Ji et al. 2019). However, accurately measuring the escape fraction remains difficult. Most of these studies yielded null or tentative detection of LyC emission. Furthermore, studies based on ground-based observations suffer from foreground contamination, resulting in overestimating the LyC escape fraction. To date, there are only several convincing detection of LyC emission in galaxies at $z \sim 3$, including *Ion2* and *Ion3* (Vanzella et al. 2016, 2018), Q1549-C25 (Shapley et al. 2016), A2218-Flanking (Bian et al. 2017), and Sunburst Arc (Rivera-Thorsen et al. 2019). In addition, the LyC escape fraction measured in individual galaxies has large uncertainty due to the opacity variations of the line of sight of IGM and galaxy ISM (Cen & Kimm 2015). Furthermore, the high LyC escape fraction measured in individual objects is not necessarily representing the LyC escape fraction of typical galaxies at the epoch of reionisation.

Studies have shown that the high-redshift galaxy luminosity function is steep at the faint end, thus sub- L^* galaxies dominate the UV emission at the epoch of reionisation. It is essential to push the LyC escape fraction measurement to faint galaxies. In this study, we measure the LyC escape fraction in a sample of Ly α emitters (LAEs) at $z \approx 3.1$ with $L \sim 0.1L^*$ in the GOODS-South field (Dickinson et al. 2003). The redshift of these LAEs have been accurately measured by the MUSE Hubble Ultra-Deep Field (HUDF) survey and the MUSE-Wide survey based on their Ly α emission lines (Japelj et al. 2017; Urrutia et al. 2018). Their LyC emission is well covered by the deep HST/WFC3 F336W images from the Hubble Deep UV Legacy Survey (HDUV, Oesch et al. 2018).

Throughout this paper, we use the following cosmological parameters: Hubble constant $H_0 = 70 \text{ km s}^{-1} \text{ Mpc}^{-1}$, dark matter density $\Omega_M = 0.30$, and dark energy density $\Omega_\Lambda = 0.70$ for a flat universe. All the magnitudes are expressed in the AB magnitude system (Oke & Gunn 1983).

2 SAMPLE SELECTION

In this study, we use the deep *HST*/WFC3 F336W images to measure the LyC escape fraction in a sample of LAEs at $z \approx 3.1$ in the GOODS-South field. We use the HST/WFC3 F336W imaging data from the HDUV survey (Oesch et al. 2018). The HDUV survey is a deep UV imaging legacy survey covering a total of area of about 100 arcmin^2 in the two GOODS fields in F275W and F336W bands. The depths of the F275W and F336W bands are 27.6 and 28.0 (5σ), respectively. The deep F275W and F336W images from the HDUV survey have been used to study the LyC escape fraction in galaxies at $z \sim 2$ and $z \sim 3$, respectively (Naidu et al. 2017; Rutkowski et al. 2017; Japelj et al. 2017). In particular, Japelj et al. (2017) studied the LyC escape fraction in a sample of galaxies at $z = 3 - 4$ selected in 9 arcmin^2 MUSE HUDF survey field using the HDUV F336W image and found the relative escape fraction $f_{\text{esc,rel}} < 0.6$ for galaxies with $0.1L^*$. Here we extend the study to a 44 arcmin^2 area using the newly published the MUSE wide survey (Urrutia et al. 2018). The MUSE-Wide survey is an integral field spectroscopic survey, largely overlaps with the HDUV in the GOODS-South field. Thanks to the VLT/MUSE integral field spectrograph (Bacon et al. 2010), this survey is

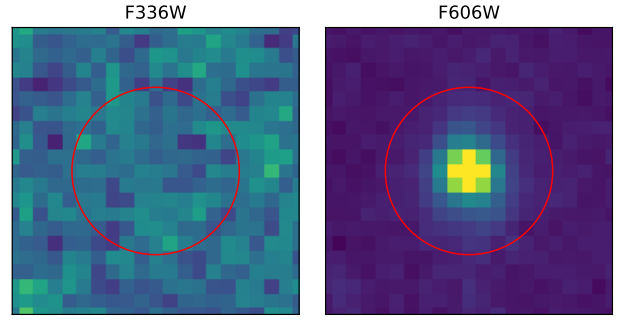


Figure 1. Stacked images for the 54 LAEs at $z = 3.1$ selected in the GOODS-S filed in *HST*/WFC3 F336W band (left) and ACS F606W band (right). The flux in each image is measured in the red circles with $0.7''$ in diameter.

able to detect galaxies without photometric pre-selection, thus it provides a high complete rate on detecting emission line galaxies. In the MUSE-Wide survey, we select LAEs in the redshift range of $z = 3.02 - 3.24$. At this redshift range, the HST WFC3/F336W filter cover the Lyman continuum at the wavelength range of 750 to 890 \AA . In this study, we only use galaxies with redshift quality greater or equal to 2 (Urrutia et al. 2018). The lower limit redshift of $z = 3.02$ corresponds to the Lyman limits at observer-frame 3684 \AA . At this wavelength the throughput of the F336W filter is less than 1%, which minimises the contamination of the flux redward of the Lyman limit.

A total of 54 Ly α emitting galaxies (LAEs) at the redshift range of $z = 3.02 - 3.24$ are selected in the GOODS-south field with deep HDUV F336W images coverage. Among them, 26 LAEs are selected from the MUSE wide survey (Urrutia et al. 2018), and 28 LAEs are from the MUSE HUDF survey (Japelj et al. 2017). Their median stellar mass is $\log(M_*/M_\odot) = 8.0$, and median dust extinction is $A_V = 0.1$. These LAEs represent a population of the galaxies with low stellar mass and young stellar population (Urrutia et al. 2018).

3 THE LYMAN CONTINUUM ESCAPE FRACTION IN LAES AT $Z=3.1$

The *HST*/WFC3 F336W image covers the LyC emission at the rest-frame wavelength of $\sim 820 \text{ \AA}$ in the LAEs at $z \approx 3.1$. None of the 54 Ly α emitting galaxies (LAEs) is detected in the F336W image at 3σ . Therefore, we try to detect and measure the LyC emission by stacking the F336W images. We generate a $10'' \times 10''$ stamp image in F336W for each individual LAE based on the galaxy coordinate measured in the F606W images. Here we do not use the galaxy coordinate from the MUSE-Wide survey, because there exist small offsets ($\sim 0.3''$) between the MUSE coordinates and the HST coordinates (Urrutia et al. 2018). The stacked F336W image is generated by combining the F336W stamp images of all 54 LAEs using the mean flux at each pixel (Figure 1). We measure the LyC flux in the F336W stacked image using a $0.7''$ diameter aperture and find that LyC flux is not detected at 3σ level. The 3σ flux upper limit in F336W band is $< 0.002 \mu\text{Jy}$, which corresponds to > 30.64 AB magnitude. We use the flux in the HST/ACS F606W image,

which corresponds to the rest-frame wavelength of 1500\AA , as an anchor point to estimate the intrinsic LyC emission at 820\AA . We use the ACS F606W images from the 3D-HST data release 4.5.1¹ (Momcheva et al. 2016). We combine the F606W images for the LAEs following the same procedure used for the F336W images (Figure 1). Then the F606W flux is measured in the final combined F606W images using a $0.7''$ diameter aperture. This aperture size is the same as used in the 3D-HST survey (Skelton et al. 2014), which includes a large fraction of the flux from the object and avoid flux from the neighbouring objects. The flux density of the F606W band is $0.074 \pm 0.001 \mu\text{Jy}$. The apparent magnitude in F606W band is 26.72 ± 0.01 AB magnitude, and the absolute magnitude at the rest-frame wavelength of 1500\AA is $M_{UV} = -18.86$, which corresponds to $0.1L^*$ at $z \sim 3$ (e.g., Bian et al. 2013).

We measure the relative LyC escape fraction f_{esc} :

$$f_{\text{esc,rel}} = \frac{L_{1500}/L_{820}}{f_{1500}/f_{820}} \times \exp(\tau_{\text{IGM},820}) \quad (1)$$

and absolute LyC escape fraction

$$f_{\text{esc}} = f_{\text{esc,rel}} \times 10^{-0.4A_{1500}} \quad (2)$$

where f_{1500}/f_{820} is the observed flux density ratio between 1500\AA and 820\AA measured in the HST F606W and F336W images. L_{1500}/L_{820} is the intrinsic luminosity density ratio between 1500\AA and 820\AA . Here, we adopt two L_{1500}/L_{820} values, $L_{1500}/L_{820} = 3$ and $L_{1500}/L_{820} = 7$, to cover a wide range of possible star formation history (e.g., Siana et al. 2007; Chisholm et al. 2019). $\exp(\tau_{\text{IGM},820}) \equiv 1/T$ is the mean IGM opacity at 820\AA at $z = 3.1$ (e.g., Madau 1995), and T is the mean IGM transmission. In this study, we adopt the Inoue et al. (2014) recipe to estimate the mean IGM opacity and find $\exp(\tau_{\text{IGM},820}) = 3.84$ at $z = 3.1$, corresponding to $T = 0.26$. A_{1500} represents the total dust extinction at 1500\AA , which is estimated from the median extinction at the V-band, $A_V = 0.18$, by adopting the Gordon et al. (2003) Small Magellanic Cloud (SMC) dust extinction curve. At last, we find that the 3σ upper limit of average LyC escape fractions in this sample of LAEs are $f_{\text{esc}} < 14\%$ and $f_{\text{esc}} < 32\%$, for $L_{1500}/L_{820} = 3$ and $L_{1500}/L_{820} = 7$, respectively.

4 PHYSICAL PROPERTIES OF THE LYMAN-ALPHA EMITTERS

We study the physical properties of the LAEs in this work by fitting their mean spectral energy distribution (SED). We obtain the mean SED by stacking the HST F435W, F606W, F775W, F814W, F850LP, F120W, F140W, and F160W images. All the images are taken from the 3D-HST data release 4.5.1 (Momcheva et al. 2016). The images from each filter are combined by following the same method that is used to combine the F336W band images. The fluxes in each of these bands are measured within an aperture of $0.7''$ in diameter. The Fitting and Assessment of Synthetic Templates (FAST) code is used to fit the mean SED (Kriek et al. 2009). We adopt the Bruzual & Charlot (2003) stellar synthesis models with a Chabrier Initial Mass Function (IMF; Chabrier

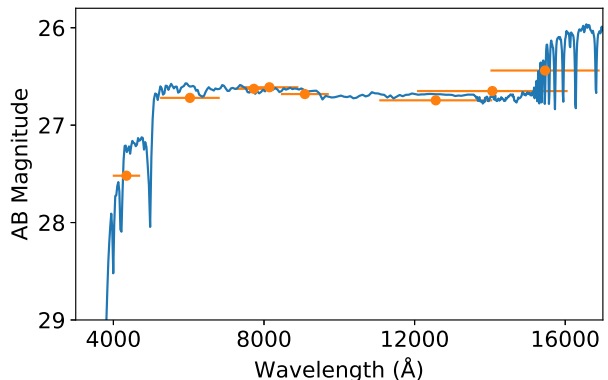


Figure 2. Best fit stellar synthesis model (blue curve) to the mean SED of the LAEs in this work in F435W, F606W, F775W, F814W, F850LP, F120W, F140W, and F160W bands (orange data points).

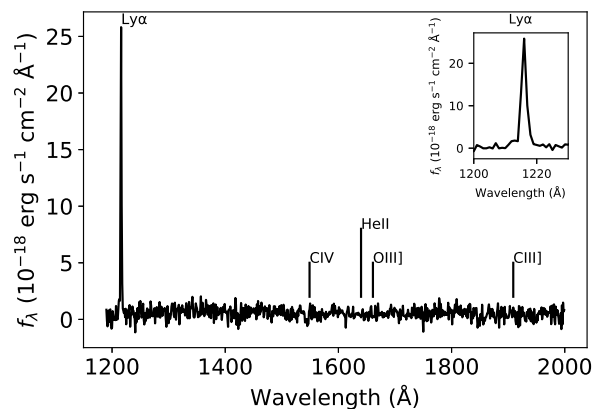


Figure 3. Composite spectrum of the LAEs whose LyC escape fraction is measured in the GOODS-South field. The strong emission line is the Ly α emission line.

2003), an SMC dust extinction curve (Gordon et al. 2003), a 0.2 solar metallicity ($Z=0.004$), and an exponentially declining star formation history. Figure 2 shows the best fit stellar synthesis model to the mean SED. We find the stellar mass of $\log(M/M_{\odot}) = 8.6$, the galaxy age of 120 Myr, and the average SFR of $4 M_{\odot} \text{ yr}^{-1}$. The average SFR and stellar mass derived from the SED fitting place these galaxies on the galaxy star formation main sequence at $z \sim 3$ (Speagle et al. 2014).

The morphology of the LAEs is compact in the stacked F606W image (Figure 1), corresponding to the rest-frame UV ($\sim 1500\text{\AA}$) images. We measure the galaxy size by fitting the stacked F606W image to a Sérsic profile using the GALFIT code (Peng et al. 2010). The angular size of the galaxy effective radius is $r_e = 0.16''$, corresponding to physical size of $r_e = 1.2 \text{ kpc}$. The Sérsic index derived from the fitting is $n = 1.37$, suggesting an exponential disk-like morphology. The mean galaxy effective radius and mass place these galaxies on the mass-size relation at $z \sim 3$ when extrapolating the relation to low mass end (e.g., van der Wel et al. 2014).

We obtain a composite spectrum of the LAEs by stacking the MUSE spectra. First, we de-redshift each MUSE spectrum to the rest-frame wavelength and re-sample spec-

¹ <https://3dhst.research.yale.edu/Data.php>

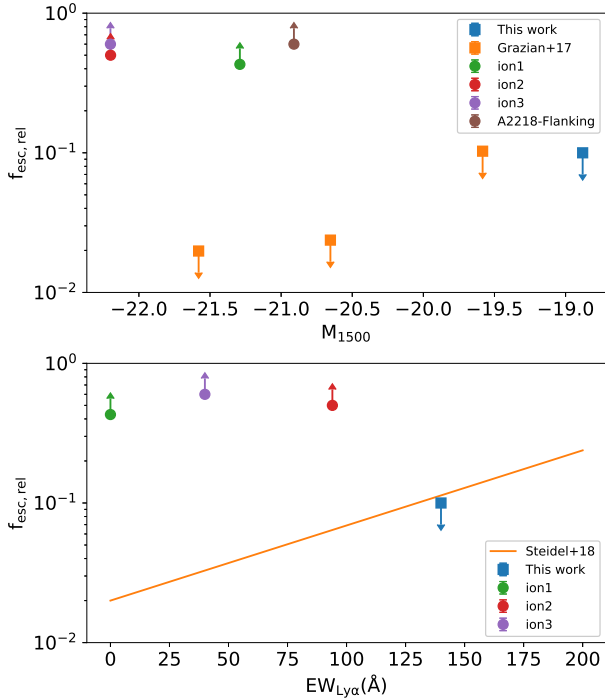


Figure 4. Relative LyC escape fraction vs absolute UV magnitude (upper panel) and EW of Ly α line (bottom panel). The squares represent the measurements from stacked images [Grazian et al. \(2017\)](#) and this work, and the solid circles represent the results from individual galaxies, *Ion1* ([Ji et al. 2019](#)), *Ion2* ([Vanzella et al. 2016](#)), *Ion3* ([Vanzella et al. 2018](#)), and A2218-Flanking ([Bian et al. 2017](#)). The orange solid line is the relation adopted from [Steidel et al. \(2018\)](#) based on the stacked spectra. All the relative LyC escape fraction has been scaled to $L_{UV}/L_{LyC} = 3$ and 1σ the upper limit.

trum to rest-frame wavelength from 1180Å to 1950Å with an interval of 1Å. The spectra were combined using the average flux density at each wavelength. Figure 3 shows the composite spectrum of the LAEs. The rest-frame equivalent width of Ly α emission is $EW_0 = 142\text{\AA}$. The high Ly α EW_0 suggests that the ages of these LAEs are young, on the order of a few times 10^7 years for a constant SFR model ([Hashimoto et al. 2017](#)). This is broadly consistent with the SED fitting results. The Ly α flux is $5.1 \times 10^{-17} \text{ erg s}^{-1} \text{ cm}^{-2}$, corresponding to a luminosity of $4.2 \times 10^{42} \text{ erg s}^{-1}$. The Ly α emission escape fraction is $\sim 60\%$ based on the SFR of $4 M_{\odot} \text{ yr}^{-1}$ ([Kennicutt 1998](#); [Verhamme et al. 2017](#)).

5 DISCUSSION

5.1 LyC emission and Galaxy Properties

The relations between the LyC escape fraction and galaxy properties have been established by both theoretical and observational studies (e.g., [Reddy et al. 2016](#); [Verhamme et al. 2017](#); [Steidel et al. 2018](#)). Galaxies with stronger Ly α emission strength, weaker interstellar absorption strength, higher [OIII]/[OII] ratio, higher star formation surface density, lower stellar mass and UV luminosity tend to have higher escape fraction (cf. [Bassett et al. 2019](#); [Ji et al. 2019](#)). Such studies help us to better understand the physical mecha-

nism(s) that drives the LyC leaking from a galaxy; extrapolation of such relations to galaxies at higher redshift can be used to predict the LyC escape in galaxies at the epoch of reionisation.

In this study, the galaxies are selected by their strong Ly α emission lines. These LAEs show high Ly α equivalent width and high Ly α escape fraction. Studies have suggested that galaxies with high LyC escape fractions commonly shows strong Ly α emission ($EW_0(\text{Ly}\alpha) > 70\text{\AA}$) and high Ly α emission line escape fraction $> 20\%$ (e.g., [Verhamme et al. 2017](#); [Kimm et al. 2019](#)). To our knowledge, the Ly α EW_0 in the composite spectrum of these LAEs is higher than all of the known LyC-leaking galaxies with $f_{\text{esc}} > 30\%$ (e.g., [Verhamme et al. 2017](#); [Vanzella et al. 2016, 2018](#)) (Figure 4). The other properties of the LAEs in this work are also in favour to having high LyC escape fraction, including lower stellar mass and UV luminosity, compared to those individual galaxies with high LyC escape fraction ($f_{\text{esc}} > 30\%$) at the similar redshift range, such as *Ion2*, *Ion3*, and A2218-Flank (Figure 4). Based on these properties, these LAEs in this study are expected to have even larger LyC escape fraction $> 30\%$. However, the non-detection of LyC emission in the stacked HST F336W image suggests a rather low ($< 14 - 32\%$) LyC escape fraction in these LAEs.

Figure 4 shows the relative LyC escape fraction vs. absolute UV magnitude and Ly α EW. The relative LyC escape fraction measured in the individual galaxies have much higher LyC escape fraction measured in the stacked images or spectra. The individual galaxies with high LyC escape fraction do not follow the relation of the LyC escape fraction and the galaxies physical properties derived from the stacking analysis based on typical $z \sim 3$ galaxies. Therefore, their high escape fractions may not represent the typical LyC escape fraction in the galaxies with similar UV luminosity and Ly α EW at $z \sim 3$. It suggests that the UV luminosity and Ly α EW may not be the best indicator for the LyC escape fraction, especially for galaxies with high LyC escape fraction. Actually, it has been found that in some of the cases the Ly α EW itself is not a good indicator of LyC escape fraction (e.g., [Guaita et al. 2016](#); [Grazian et al. 2017](#); [Ji et al. 2019](#)), because the Ly α photons can escape via pure radiative transfer effects even in a relatively high H I column density (e.g., $N_{\text{HI}} > 10^{20} \text{ cm}^{-2}$), which is completely optically thick for the LyC radiation (e.g., [Verhamme et al. 2006](#)). Therefore, the detailed Ly α profile, such as the separation of the blue and red peaks and leaking of the Ly α at systematic redshift, can also provide crucial information on the LyC leaking.

5.2 Systematic Uncertainties of LyC Escape Fraction

Our LyC escape fraction measurement also faces large systematic uncertainties as follows:

- Galaxy viewing angle: Studies have shown that the LyC photons can only escape from chimneys and holes in the ISM of galaxy caved by the supernovae and other stellar feedbacks (e.g., [Heckman et al. 2011](#)). This indicates that the leaking LyC photons can only be detected in a small fraction of the solid angle of galaxies, and the LyC escape fraction measurements highly depends on the viewing angle of the galaxy. It can cause a large uncertainty on the LyC

escape fraction based on the measurements in a small sample of galaxies. Cen & Kimm (2015) suggested that it requires to stack at least 100 galaxies to reduce the LyC escape fraction uncertainty down to 20%.

2. IGM transmission: LyC escape fraction measurement also depends on the IGM transmission. Japelj et al. (2017) found that the $z = 3.1$ IGM transmission in F336W band at a random line of sight is $0.26^{+0.30}_{-0.25}$. For a sample of 54 galaxies, the uncertainty of the IGM transmission is about 15%.

3. The spatial offset between the LyC and UV light centroids: The stacking strategy relies on the assumption that the LyC emission has the same location as the UV emission at 1500\AA . Observations of gravitational lensed system, Sunburst, indicate that the LyC emission only emerges in some of the star-forming knots and varies significantly from one knot to other knots (Vanzella et al. 2019; Rivera-Thorsen et al. 2019). Therefore, the LyC and UV centroid positions are not necessary always well-aligned. The LyC signal will be diluted due to such misalignment during the stacking process, and the LyC escape fraction can be significantly underestimated.

6 CONCLUSIONS

In this letter, we study the LyC escape fraction in a sample of LAEs. These LAEs represent a population of compact young dwarfs at $z = 3.1$. We summarise the main results of this work as follows:

1. A sample of 54 Ly α emitters (LAEs) at $z = 3.02 - 3.24$ are selected from the MUSE Hubble Ultra Deep Field (HUDF) and MUSE MUSE-Wide integral field spectroscopic survey in the GOODS-South field based on their prominent Ly α emission.

2. We fit stellar synthesis models to the composite SED of these LAEs and find the stellar mass of $\log(M/M_{\odot}) = 8.6$, the age of 120 Myr, and the SFR of $3.2 M_{\odot} \text{ yr}^{-1}$.

3. The galaxy size at the UV wavelength measured in the stacked HST F606W image is 1.2 kpc, and the rest-frame equivalent width of the Ly α emission is 142\AA , which is measured in the composite MUSE spectra of these LAEs.

4. The LyC emission of these LAEs is not detected at 3σ level in the stacked HDUV deep HST F336W image, covering the rest-frame wavelength of 820\AA in these LAEs. The upper limits of LyC escape fraction are $f_{\text{esc}} < 14\%$ and $f_{\text{esc}} < 32\%$, for $L_{1500}/L_{820} = 3$ and $L_{1500}/L_{820} = 7$, respectively.

5. Such low LyC escape fraction of these LAEs suggests that the LyC leaking galaxies at $z \sim 3$ do not follow the relation of LyC escape fraction and galaxy properties, including UV luminosity and Ly α EW. It implies that the UV luminosity and Ly α EW are not the best properties to predict the LyC escape fraction, particularly for galaxies with high escape fractions.

ACKNOWLEDGEMENTS

We thank the MUSE GTO, HDUV, and 3D-HST teams to release their data set to public, making this work possible. We thank Dr. J. Japelj to share the detailed information on

the LAEs in the MUSE Hubble Ultra Deep Field Survey. We thank the anonymous referee for providing constructive comments and help in improving the manuscript.

REFERENCES

- Atek H., et al., 2015, *ApJ*, **800**, 18
Atek H., Richard J., Kneib J.-P., Schaerer D., 2018, *MNRAS*, **479**, 5184
Bañados E., et al., 2018, *Nature*, **553**, 473
Bacon R., et al., 2010, in *Ground-based and Airborne Instrumentation for Astronomy III*. p. 773508, doi:10.1117/12.856027
Bassett R., et al., 2019, *MNRAS*, **483**, 5223
Bian F., et al., 2013, *ApJ*, **774**, 28
Bian F., et al., 2015, *ApJ*, **806**, 108
Bian F., Fan X., McGreer I., Cai Z., Jiang L., 2017, *ApJ*, **837**, L12
Boutsia K., Grazian A., Giallongo E., Fiore F., Civano F., 2018, *ApJ*, **869**, 20
Bouwens R. J., et al., 2015a, *ApJ*, **803**, 34
Bouwens R. J., Illingworth G. D., Oesch P. A., Caruana J., Holwerda B., Smit R., Wilkins S., 2015b, *ApJ*, **811**, 140
Bouwens R. J., Smit R., Labbé I., Franx M., Caruana J., Oesch P., Stefanon M., Rasappu N., 2016, *ApJ*, **831**, 176
Bouwens R. J., Oesch P. A., Illingworth G. D., Ellis R. S., Stefanon M., 2017, *ApJ*, **843**, 129
Bruzual G., Charlot S., 2003, *MNRAS*, **344**, 1000
Cen R., Kimm T., 2015, *ApJ*, **801**, L25
Chabrier G., 2003, *PASP*, **115**, 763
Chevallard J., et al., 2018, *MNRAS*, **479**, 3264
Chisholm J., Rigby J. R., Bayliss M., Berg D. A., Dahle H., Gladsters M., Sharon K., 2019, *ApJ*, **882**, 182
Cooke J., Ryan-Weber E. V., Garel T., Díaz C. G., 2014, *MNRAS*, **441**, 837
Dickinson M., Giavalisco M., GOODS Team 2003, in Bender R., Renzini A., eds, *The Mass of Galaxies at Low and High Redshift*. p. 324 (arXiv:astro-ph/0204213), doi:10.1007/10899892_78
Fan X., Carilli C. L., Keating B., 2006a, *ARA&A*, **44**, 415
Fan X., et al., 2006b, *AJ*, **132**, 117
Fletcher T. J., Robertson B. E., Nakajima K., Ellis R. S., Stark D. P., Inoue A., 2018, arXiv e-prints,
Giallongo E., et al., 2015, *A&A*, **578**, A83
Gordon K. D., Clayton G. C., Misselt K. A., Landolt A. U., Wolff M. J., 2003, *ApJ*, **594**, 279
Grazian A., et al., 2017, *A&A*, **602**, A18
Guaita L., et al., 2016, *A&A*, **587**, A133
Hashimoto T., et al., 2017, *A&A*, **608**, A10
Heckman T. M., et al., 2011, *ApJ*, **730**, 5
Inoue A. K., Shimizu I., Iwata I., Tanaka M., 2014, *MNRAS*, **442**, 1805
Itoh R., et al., 2018, *ApJ*, **867**, 46
Izotov Y. I., Schaerer D., Thuan T. X., Worseck G., Guseva N. G., Orlitová I., Verhamme A., 2016a, *MNRAS*, **461**, 3683
Izotov Y. I., Orlitová I., Schaerer D., Thuan T. X., Verhamme A., Guseva N. G., Worseck G., 2016b, *Nature*, **529**, 178
Japelj J., et al., 2017, *MNRAS*, **468**, 389
Ji Z., et al., 2019, arXiv e-prints, p. arXiv:1908.00556
Kakiichi K., et al., 2018, *MNRAS*, **479**, 43
Kennicutt Jr. R. C., 1998, *ARA&A*, **36**, 189
Kimm T., Blaizot J., Garel T., Michel-Dansac L., Katz H., Rosdahl J., Verhamme A., Haehnelt M., 2019, *MNRAS*, **486**, 2215
Kriek M., van Dokkum P. G., Labbé I., Franx M., Illingworth G. D., Marchesini D., Quadri R. F., 2009, *ApJ*, **700**, 221
Leitert E., Bergvall N., Hayes M., Linné S., Zackrisson E., 2013, *A&A*, **553**, A106
Leitherer C., Hernandez S., Lee J. C., Oey M. S., 2016, *ApJ*, **823**, 64

- Livermore R. C., Finkelstein S. L., Lotz J. M., 2017, *ApJ*, **835**, 113
- Madau P., 1995, *ApJ*, **441**, 18
- Matsuoka Y., et al., 2018, *ApJ*, **869**, 150
- McGreer I. D., Fan X., Jiang L., Cai Z., 2018, *AJ*, **155**, 131
- Momcheva I. G., et al., 2016, *ApJS*, **225**, 27
- Naidu R. P., et al., 2017, *ApJ*, **847**, 12
- Naidu R. P., Tacchella S., Mason C. A., Bose S., Oesch P. A., Conroy C., 2019, arXiv e-prints, p. [arXiv:1907.13130](https://arxiv.org/abs/1907.13130)
- Nestor D. B., Shapley A. E., Steidel C. C., Siana B., 2011, *ApJ*, **736**, 18
- Nestor D. B., Shapley A. E., Kornei K. A., Steidel C. C., Siana B., 2013, *ApJ*, **765**, 47
- Oesch P. A., et al., 2018, *ApJS*, **237**, 12
- Oke J. B., Gunn J. E., 1983, *ApJ*, **266**, 713
- Pawlik A. H., Schaye J., van Scherpenzeel E., 2009, *MNRAS*, **394**, 1812
- Peng C. Y., Ho L. C., Impey C. D., Rix H.-W., 2010, *AJ*, **139**, 2097
- Planck Collaboration et al., 2016, *A&A*, **596**, A108
- Reddy N. A., Steidel C. C., Pettini M., Bogosavljević M., Shapley A. E., 2016, *ApJ*, **828**, 108
- Rivera-Thorsen T. E., et al., 2019, arXiv e-prints,
- Robertson B. E., et al., 2013, *ApJ*, **768**, 71
- Rutkowski M. J., et al., 2016, *ApJ*, **819**, 81
- Rutkowski M. J., et al., 2017, *ApJ*, **841**, L27
- Schenker M. A., Ellis R. S., Konidaris N. P., Stark D. P., 2014, *ApJ*, **795**, 20
- Schroeder J., Mesinger A., Haiman Z., 2013, *MNRAS*, **428**, 3058
- Shapley A. E., Steidel C. C., Pettini M., Adelberger K. L., Erb D. K., 2006, *ApJ*, **651**, 688
- Shapley A. E., Steidel C. C., Strom A. L., Bogosavljević M., Reddy N. A., Siana B., Mostardi R. E., Rudie G. C., 2016, *ApJ*, **826**, L24
- Siana B., et al., 2007, *ApJ*, **668**, 62
- Siana B., et al., 2015, *ApJ*, **804**, 17
- Skelton R. E., et al., 2014, *ApJS*, **214**, 24
- Speagle J. S., Steinhardt C. L., Capak P. L., Silverman J. D., 2014, *ApJS*, **214**, 15
- Stark D. P., Ellis R. S., Ouchi M., 2011, *ApJ*, **728**, L2
- Steidel C. C., Pettini M., Adelberger K. L., 2001, *ApJ*, **546**, 665
- Steidel C. C., Bogosavljević M., Shapley A. E., Reddy N. A., Rudie G. C., Pettini M., Trainor R. F., Strom A. L., 2018, *ApJ*, **869**, 123
- Tang M., Stark D., Chevallard J., Charlot S., 2018, arXiv e-prints, p. [arXiv:1809.09637](https://arxiv.org/abs/1809.09637)
- Urrutia T., et al., 2018, arXiv e-prints,
- Vanzella E., et al., 2010, *ApJ*, **725**, 1011
- Vanzella E., et al., 2016, *ApJ*, **825**, 41
- Vanzella E., et al., 2018, *MNRAS*, **476**, L15
- Vanzella E., et al., 2019, *MNRAS*, p. 2218
- Vasei K., et al., 2016, *ApJ*, **831**, 38
- Verhamme A., Schaerer D., Maselli A., 2006, *A&A*, **460**, 397
- Verhamme A., Orlitová I., Schaerer D., Izotov Y., Worseck G., Thuan T. X., Guseva N., 2017, *A&A*, **597**, A13
- van der Wel A., et al., 2014, *ApJ*, **788**, 28

This paper has been typeset from a $\text{\TeX}/\text{\LaTeX}$ file prepared by the author.